Journal Name

ARTICLE

Direct and Continuous Synthesis of VO_2 Nanoparticles

M. J. Powell,[a] P. Marchand,[a] C. J. Denis,[a] J. C. Bear,[b] J. A. Darr,[a] and I. P. Parkin[a†]

Received 00th January 20xx,
Accepted 00th January 20xx

DOI: 10.1039/x0xx00000x

www.rsc.org/

Abstract: Monoclinic VO_2 nanoparticles are of interest due to the material's thermochromic properties, however, direct synthesis routes to VO_2 nanoparticles are often inaccessible due to the high synthesis temperatures or long reaction times required. Herein, we present a two-step synthesis route for the preparation of monoclinic VO_2 nanoparticles using Continuous Hydrothermal Flow Synthesis (CHFS) followed by a short post heat treatment step. A range of particle sizes, particle size was dependent on synthesis conditions, were produced (average particle size was in the range 50 to 200 nm) by varying reaction temperatures and the residence times in the process. The nanoparticles were characterised by powder X-ray diffraction, Raman and UV/Vis spectroscopy, transmission electron microscopy (TEM), scanning electron microscopy (SEM) and differential scanning calorimetry (DSC). The nanoparticles were highly crystalline with rod and sphere-like morphologies present in TEM micrographs, with the size of both the rod and spherical particles being highly dependent on both reaction temperature and residence time. SEM micrographs showed the surface of the powders produced from the CHFS process to be highly uniform. The samples were given a short post synthesis heat treatment to ensure that they were phase pure monoclinic VO_2, which led to them exhibiting a large and reversible switch in optical properties (at near-IR wavelengths), which suggests that if such materials can be incorporated into coatings or in composites, they could be used for fenestration in architectural applications.

Introduction

Anthropogenic induced climate change is rapidly altering the planet's temperature, weather, rain cycles and sea level.[1, 2] This is already causing an increased risk of droughts, floods, famines and the associated diseases this would entail, as well as an increased rate of extinction among vulnerable species.[3] In order to combat this challenge, it is necessary to take a holistic view of the energy infrastructure, including the design of buildings to ensure that there are both carbon neutral energy sources and the maximum possible energy efficiency. Fenestration has become an increasingly researched area to this end, as buildings consume ca. 30-40% of all the energy generated each year,[4] with a large proportion of this energy being lost through the windows in a building. There is thus a requirement to develop energy saving materials that can change their properties in accordance with the wider environment. These so called "smart" materials for example, could allow a reduction in energy consumption by being transmissive to infra-red radiation when cold, and reflective of infra-red radiation when hot, alleviating some of the need for air-conditioning and heating within buildings.

Vanadium (IV) oxide has several different stable phases, these are termed VO_2 (A),[5] (B),[6, 7] (M) and (R).[8, 9] The (A) and (B) phases of VO_2 have shown promise for Li-ion batteries, with the (B) phase extensively researched due to the ability to intercalate lithium ions with the crystal structure.[10, 11] VO_2 (M) undergoes a reversible phase transition to VO_2 (R) when it reaches ~68 °C (in the undoped form), it undergoes a phase transition from monoclinic (semi-conductor) to rutile (semi-metallic) crystal structure. The phase change that occurs is abrupt [known as metal-to-semiconductor transition (MST)] and results in a large change in both the electrical resistance and the optical properties in the near infrared region (from ca. 860 to 2500 cm^{-1}). The monoclinic form of vanadium dioxide, VO_2 (M), behaves as a semiconductor and is passive to near IR wavelengths, whereas the rutile, VO_2 (R), is semi-metallic in nature and highly reflective to near IR wavelengths. Due to these properties, VO_2 has tremendous potential to be used in thermochromic windows,[12-14] switches for computing[15] and sensor applications, amongst others.[16] Due to the complex phase diagram of VO_2, it is difficult to directly synthesise VO_2 (M),[17] and as such there are no design rules for the synthesis of VO_2 (M) nanoparticles.

In thermochromic applications, VO_2 coatings have the potential to radically reduce the amount of energy required to keep buildings at an ambient temperature, which would return substantial savings in energy.[18] The use of such materials in architectural applications could lead to a large reduction in energy consumption due to air conditioning and heating loads within buildings, with the subsequent reduction in CO_2 emissions further helping to combat anthropogenically induced climate change. However, due to the yellow/brown colour of

[a] *University College London, Department of Chemistry, Materials Chemistry Centre, 20 Gordon Street, London, WC1H 0AJ*
[b] *College of Engineering, Swansea University, Singleton Park, Swansea, SA2 8PP*
† i.p.parkin@ucl.ac.uk
Electronic Supplementary Information (ESI) available: [details of any supplementary information available should be included here]. See DOI: 10.1039/x0xx00000x

VO_2 films, and the fact that the films can fracture over time due to stress, thermochromic VO_2 has yet to be applied industrially. These issues could be overcome by development of nanoscale VO_2 powders. If these particles can be made ca. 50 nm or smaller, it may be possible to spin-coat them into films that alleviates the aesthetic issues with traditional VO_2 thin films as the particles will be poor scatterers of visible wavelengths.[19] For such applications on an industrial scale, it is necessary to develop continuous and scalable methods of synthesis that have consistent and controlled conditions. Many of the current methods to make nanoparticles are not always consistent in term of reproducibly at scale, or require long reaction times with little or no control over particle properties, e.g. batch hydrothermal processes for monoclinic VO_2 can take several days to yield phase pure materials.[20, 21] Sol-gel methods for producing VO_2 require high reaction temperatures (~800 °C) and need to be annealed under vacuum to achieve the desired monoclinic to rutile switching behaviour.[22, 23] Other solution based routes, such as refluxing to reduce V_2O_5 into VO_2, suffer from difficulties in scaling for industrial applications.[24, 25]

Continuous hydrothermal flow synthesis (CHFS) is a direct, reproducible and scalable method for the production of nanoparticles. In CHFS, nanoparticles are rapidly formed upon mixing of an ambient temperature stream of metal precursor salts with a stream of supercritical (or superheated) water within an engineered mixer which prevents blockages. Typically, metal oxides are formed in the process very rapidly formed by hydrolysis and subsequent dehydration of the metal salt.[26] The use of CHFS allows for the scalable synthesis of materials,[27] while also alleviating the dependence on solvents with high volatile organic contents (VOCs) common in batch reactions.[28]

Herein, we describe the direct synthesis of monoclinic VO_2 nanoparticles in a CHFS process. The nanoparticles were synthesised from a vanadium(IV) precursor solution, obtained by the reduction of ammonium metavanadate (NH_4VO_3) in the presence of oxalic acid ($H_2C_2O_4$). The effects of reaction temperature and residence time on particle size, morphology and phase purity were investigated by powder X-ray diffraction, Raman spectroscopy and transmission electron microscopy. The thermochromic properties of the synthesised nanoparticles were determined by variable temperature UV/Vis spectroscopy.

Experimental

Starting materials

Vanadium metavanadate (NH_4VO_3, 99% purity) and oxalic acid ($H_2C_2O_4$, 99% purity) were used to synthesise the vanadium (IV) precursor solution. The reagents were bought from Sigma-Aldrich UK and were used without further purification.

Preparation of precursor solution

Ammonium metavanadate (23.40 g, 0.2 mol) and oxalic acid (50.42 g, 0.4 mol) were dissolved in 2.0 L of deionised water. The solution was stirred at 25 ºC for 4 hours, forming a deep blue solution, which was then left to age overnight.[29]

Synthesis of nanoparticles by Continuous Hydrothermal Flow Synthesis (CHFS)

In the CHFS process, nanoparticles form upon mixing a feed of supercritical (or superheated) water with an ambient-temperature stream of aqueous metal salts. This is usually carried out using a particular reactor (mixer) arrangement, resulting in rapid conversion of the metal salts into metal oxides *via* instantaneous hydrolysis and dehydration.[30] Figure 1 shows a schematic diagram of the CHFS process used in the production of the VO_2 nanoparticles presented in this work. Three high-pressure diaphragm pumps P-1 to P-3 (Milton Roy, Primeroyal K) were used to supply reagents and water to the process. The outputs of each of the pumps are identified as Q_{sw} (volumetric flow rate of preheated water issuing from P-1), Q_p (combined volumetric flow rate of metal salt precursor and DI water issuing from P-2 and P-3, respectively). Pump P-1 was used to supply a flow of deionised water, which was heated to 450 °C at a pressure of 24.1 MPa (*i.e.* above the critical point of water, T_C = 374 °C and P_C = 22.1 MPa) by an electrical heater arrangement (7 kW). A flow of aqueous metal precursor supplied by pump P-2 was diluted by mixing with a deionised water feed supplied by pump P-3, in a T-piece. The combined feed was then mixed with the supercritical water feed in a confined jet mixer (CJM) as described elsewhere.[30] The newly formed nanoparticles remained at reaction temperature for a particular 'residence' time, before being cooled by passing through a pipe-in-pipe heat exchanger. The cooled nanoparticle slurry was then collected in an open beaker at 25 ºC after passing through a back pressure regulator (TESCOM model 26-1762-24-194) valve. The solids were recovered from solution by centrifugation and washing followed by dialysis for 24 hours. The cleaned wet solids were finally freeze-dried (Virtis Genesis 35XL) by slowly heating from -40 °C to 25 °C over 24 h under vacuum of <100 mTorr. The VO_2 nanoparticles formed from the hydrothermal process were post annealed to ensure that they were indeed phase pure monoclinic VO_2. This was done as follows; 0.5g of a sample was placed in a tube furnace and heated to 600 °C for 2 hours (ramp rate: 25 °C/min) under an N_2 atmosphere (BOC, 99.9%), before being left to cool to room temperature.

Sample ID	Mixing Temp (°C)	Q_{sw} /mL min^{-1}	Q_p /mL min^{-1}	Residence time /s	[VO_2] precursor /mol L^{-1}
V-1	335	80	80	22	0.5
V-2	356	76	62	22	0.5
V-3	375	80	50	20	0.5
V-4	357	64	52	27	0.5

Table 1: Synthesis conditions and sample identifiers for VO_2 nanoparticles produced by continuous hydrothermal flow synthesis. $\mathbf{Q_{sw}}$ is the pressure of the DI water from pump 1, $\mathbf{Q_p}$ is the pressure of the combined DI water and precursors from pumps 2 and 3. The residence time and mixing temperature were altered by changing the pressure on the pumps ($\mathbf{Q_{sw}}$ and $\mathbf{Q_p}$). Heater set point was 450 °C in all cases

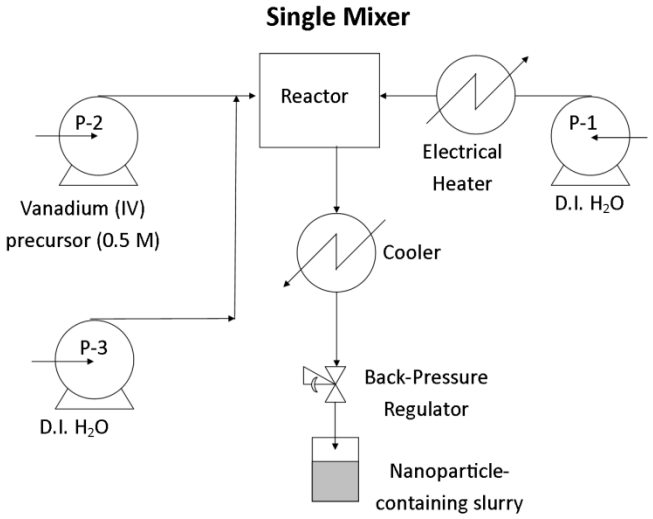

Figure 1: Schematic diagram of CHFS process used to produce VO_2 nanoparticles, flow rates and reaction temperatures can be found in Table 1.

Sample descriptions and details are summarised in Table 1. Heater set point was 450 °C in all cases.

Characterisation

X-ray diffraction (XRD) studies were carried out using a Stoe (Mo) StadiP diffractometer. The instrument operates with a Mo X-ray source (Mo tube 50 kV 30 mA), monochromated (Pre-sample Ge (111) monochromator selects Kα1 only) and a Dectris Mython 1k silicon strip detector covering 18° 2θ. Samples were run in transmission mode, with the sample being rotated in the X-ray beam. The diffraction patterns obtained were compared with database standards. Raman spectroscopy was carried out using a Renishaw 1000 spectrometer equipped with a 633 nm laser. The Raman system was calibrated using a silicon reference. UV/vis spectroscopy was performed using a Perkin Elmer Lambda 950 UV/Vis/NIR Spectrophotometer. The spectra were recorded via diffuse reflectance, with the samples being deposited onto microscope slides. Heating of samples in the UV/Vis spectrometer was achieved by an aluminium temperature cell controlled by RS cartridge heaters, Eurotherm temperature controllers and k-type thermocouples. A *Labsphere* reflectance standard was used as reference in the UV/vis measurements. Transmission electron microscopy (TEM) images were obtained using a TEM Jeol 2100 with a LaB_6 source operating at an acceleration voltage of 200 kV. Micrographs were recorded on a Gatan Orius Charge-coupled device (CCD). The powders were sonicated and suspended in methanol and drop-casted onto a 400 Cu mesh lacey carbon film grid (Agar Scientific Ltd.) for TEM analysis. Scanning electron microscopy (SEM) was carried out using a Jeol JSM-6700F and secondary electron image on a Hitachi S-3400N field emission instruments (20 KV) and the Oxford software INCA. Differential scanning calorimetry measurements were taken on a Netzsch Jupiter DSC/TGA, samples were heated to 90 °C in air (ramp rate 10 °C min^{-1}).

Results and discussion

Nanoparticles of VO_2 were synthesised by a continuous hydrothermal flow synthesis (CHFS) technique. The nanoparticles were formed from a vanadium (IV) precursor solution, which was the result of the reduction of ammonium metavanadate by oxalic acid, with the vanadium being reduced from (V) to (IV). The dark blue solution formed from this reaction was used as the VO_2 precursor for all subsequent reactions. The accepted decomposition pathway for the metal carboxylate is shown below in equations (1), (2) and (3).[31, 32] As the VO_2 product is solvated, it is generally assumed to be positively charged.

$$2\ NH_4VO_3 + 4\ H_2C_2O_4 \rightarrow (NH_4)_2[(VO)_2(C_2O_4)_3] + 2\ CO_2 + 4\ H_2O \quad (1)$$

$$(NH_4)_2[(VO)_2(C_2O_4)_3] \rightarrow 2\ VOC_2O_4 + 2\ NH_3 + CO + CO_2 + H_2O \quad (2)$$

$$VOC_2O_4 \rightarrow VO_2 + CO + CO_2 \quad (3)$$

The XRD patterns for the as-formed VO_2 nanoparticles are shown in Figure 1(a). When compared with an ICSD VO_2 monoclinic standard (ICSD 34033), a number of peaks were shifted, as well as some additional peaks observed in the data matched to VO_2 (B) (ISCD 199). This suggests that the as-synthesised nanoparticles were a mixture of VO_2 (B) and (M) phases.[6, 33] The sample showing the closest match to the VO_2 (M) reference was sample V-3, which was synthesised at the highest calculated mixing temperature of 375 °C. Comparing all the XRD patterns, the formation of the VO_2 (M) phase was clearly favoured by an increase in reaction temperature. An increase in residence time did not appear to influence the phase of the as-synthesised materials. Whilst phase-pure monoclinic VO_2 was not be produced directly from the CHFS process in these experiments, the formation of predominantly monoclinic VO_2 is observed at a residence time of only 20 s. VO_2 (M) nanoparticles have been previously made using batch hydrothermal techniques, with reaction times between 12-48 hours, so this is a significant reduction in reaction times (a factor of 2000-4000 times faster).[33-35] Under the continuous hydrothermal reactor configuration used in this work, the maximum achievable residence time was limited to 27 s. Examination of the XRD patterns for samples V-2 and V-4 show many variations, Figure 2(a). There is a large difference in intensity of the peak at 12.7° (001), with V-2 showing a peak which cannot be defined as monoclinic VO_2 whereas V-4 shows a peak much closer to the monoclinic value. The peak at 25.7° (022) shows higher definition in V-4 than V-2. This suggests that residence time can affect the phase purity of the sample, however, the difference in residence time is very small (5 s) so meaningful conclusions cannot be drawn from these data. An increase in residence time, with a high reaction temperature (375 °C or higher), could afford the formation of phase-pure VO_2 (M).

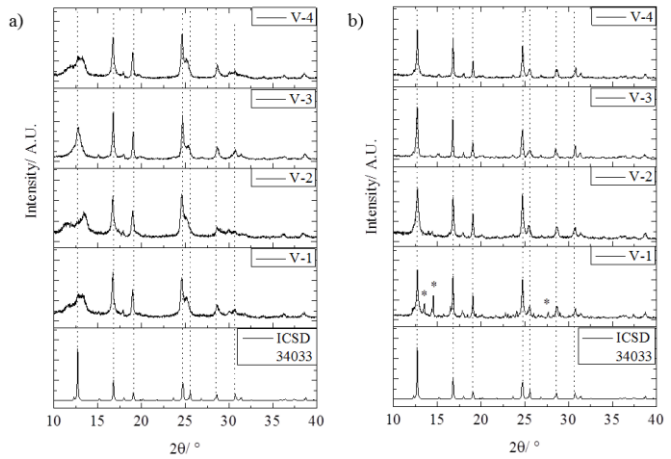

Figure 1: XRD patterns for a) samples as synthesised from the CHFS and b) samples after post-annealing at 600 °C for 2 hours under a nitrogen atmosphere. All samples are compared with an ICSD VO_2 monoclinic standard (ICSD 34033). Additional peaks in the post annealed samples are highlighted with a *. Mixing temperatures and residence times for samples are: V-1 = 335 °C and 22 s, V-2 = 356 °C and 22 s, V-3 = 375 °C and 20 s and V-4 = 357 °C and 27 s. (Mo kα: λ = 0.70926 Å)

To ensure phase pure VO_2 (M) was formed, the as-prepared materials were heat-treated at 600 °C under a nitrogen atmosphere (BOC, 99.9%). **Figure 2(b)** shows the XRD patterns for samples after heat-treatment. Samples V-2, V-3 and V-4 showed reflections only for VO_2 (M) after heat-treatment. Sample V-1, however, showed some additional reflections, suggesting that another impurity phase of vanadium oxide was present. Vanadium oxides have a complex phase diagram, with many mixed vanadium oxidation (Magneli) phases possible.[36, 37]

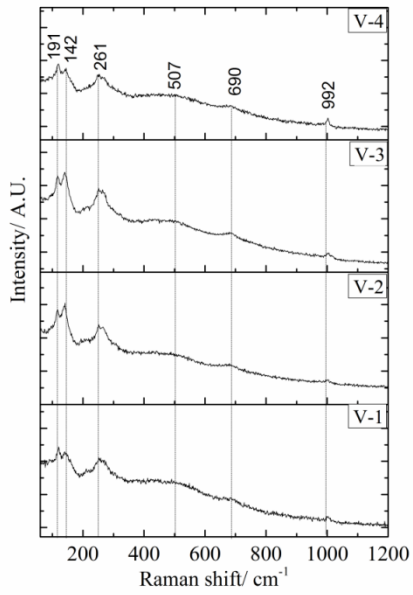

Figure 2: Raman spectra for heat-treated VO_2 samples. All bands present in the spectra are attributed to monoclinic VO_2. (Laser wavelength= 633 nm)

Sample	Mixing Temp (°C)	Residence Time (s)	Mean Particle Size (nm) Spherical	Rod Length	Rod Width
V-1	335	22	46.3 (±13.1)	239.9 (±55.2)	68.3 (±9.7)
V-2	356	22	193.4 (±38.9)	425.3 (±49.8)	35.3 (±5.2)
V-3	375	20	131.3 (±49.5)	312.8 (±70.2)	33.1 (±4.3)
V-4	357	27	131.9 (±32.4)	159.8 (±32.4)	54.3 (±11.2)

Table 2: Mean particle sizes for spherical and rod-like particles observed in VO_2 nanoparticles synthesised from continuous hydrothermal flow synthesis after heat treatment. Particle sizes obtained from TEM micrographs.

Raman spectroscopy was performed on all samples to confirm the presence of VO_2 (M) at the surface of the powders.

Figure 2 shows the Raman spectra for all samples. The bands in the data could be attributed to monoclinic VO_2, with no other phases of VO_2 being observed.[38] All the monoclinic VO_2 bands are within ± 2 cm^{-1} of literature values.[39, 40] Taken together with the XRD data in **Figure 2(b)**, this suggests that the heat-treated samples were phase-pure monoclinic VO_2.

TEM was used to examine the morphology of the nanoparticles after heat-treatment. Two distinct morphologies were observed, as shown in **Figure 5**; a spherical-like and rod-like particle formation. All samples displayed both rod-like and sphere-like particles in the TEM images. Both of these morphologies were previously reported for hydrothermal syntheses.[35, 41-43] It is unusual for both morphologies to be present in the same sample. The spherical particles also show signs of coarsening for samples V-3 and V-4 [**Figure 5 (c) and (d)**] with the particles becoming more rectangular as a result. This is also seen in the size distribution of the particles (Table 2).

The standard deviations for particle size are large for all samples, especially for sample V-2. This suggests that the growth rate of the particles is strongly linked to the residence time, with longer residence times leading to larger particle sizes.

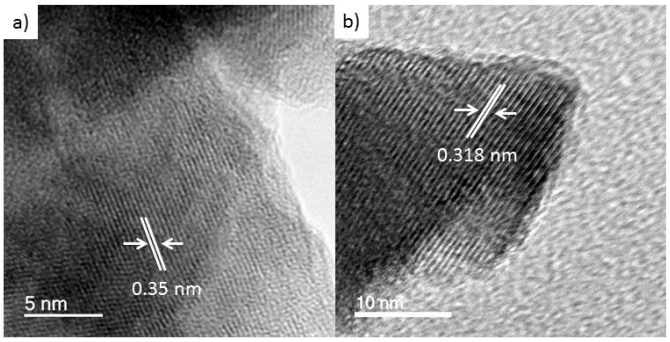

Figure 4: a) High resolution TEM micrographs of the as synthesised VO_2 nanoparticles from continuous hydrothermal flow synthesis (CHFS), the lattice fringe d-spacing was 0.350 nm which was matched to the VO_2 (B) (110) plane and **b)** High resolution TEM image of VO_2 particle after post annealing for 2 hours at 600 °C under nitrogen atmosphere. The lattice fringe d-spacing was 0.318 nm which was matched to the (011) plane of VO_2 (M).

The sintering present in the TEM images is attributed to the heat-treatment. The rod-like particles tended to be aggregated, e.g. sample V-1 [**Figure 5 (a)**] had a highly ordered orientation of the rod-like particles, where the rods appeared to be aligned in a similar direction. Sample V-2 was synthesised at a higher reaction temperature, but had a similar residence time of ~22 seconds. **Figure 5 (b)** shows a typical rod-like structure for this sample. The rods in sample V-2 have a smaller diameter but greater length than the rods in sample V-1 as shown in table 2. This is attributed to higher reaction temperatures resulting in faster growth rates. Sample V-3, **Figure 5 (c)** shows an intermediate rod-like structure to samples V-2 and V-4, this suggests that both temperature and residence time have a large effect on the growth rate and structure of the nanoparticles. Sample V-4 was synthesised at the same reaction temperature as V-2, with an increased residence time of ~27 seconds. As shown in **Figure 5 (d),** this increase in residence time led to an increase in the width, and a decrease in length, of the rod-like particles. Both samples V-2 and V-4 had a wide distribution in the width and diameter of the rod-like particles.

Scanning electron microscopy (SEM) micrographs were also obtained for the synthesised samples (**Figure 6**). As shown in Figure 6 a) and b) the as-synthesised nanoparticles had the same morphology displayed in the post-heat treated samples. This suggests that the heat treatment did not affect the crystal structure, but did cause a phase change to monoclinic VO_2. The effect of residence time can be clearly shown in these images, with samples V-1, V-3 and V-4 all showing longer needle like formations, whilst sample V-2 shows more stunted growth with rod-like formations. The large surface area of these particles is also apparent in these images, with many rod/needle like particles present in the SEM images for all the samples synthesised. It can also be seen that the surface for all of the samples is highly uniform, which shows the ability of the CHFS process to produce high quality powders at large scales.

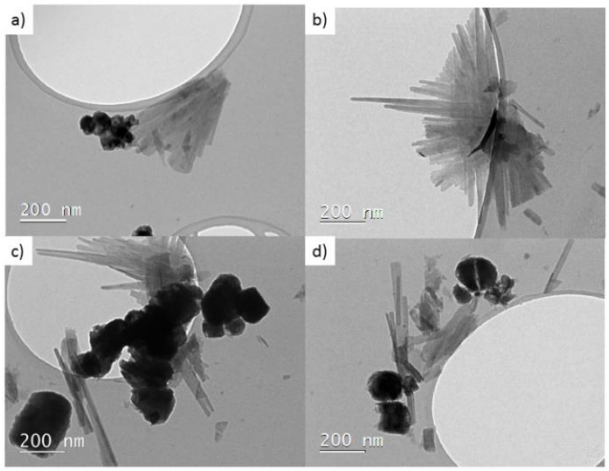

Figure 5: Transmission Electron Microscopy images for VO_2 nanoparticles: **a)** Spherical and rod-like VO_2 particles for sample V-1 **b)** Close up image of rod-like particles for sample V-2 **c)** Close-up image of spherical and rod-like particles for sample V-3 **d)** Spherical and rod-like particles in sample V-4. All samples shown have been post annealed at 600 °C for 2 hours.

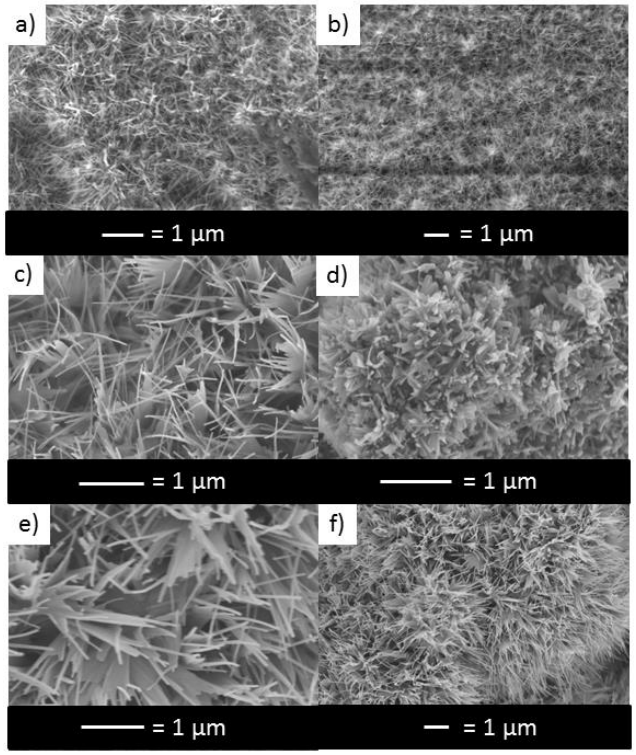

Figure 6: SEM micrographs for samples a) and b) morphology of as synthesised VO_2 powders c) V-1, d) V-2, e) V-3 and f) V-4 morphologies after post annealing. In all samples needle and rod-like particles are present, with the surface of the samples shown to be highly uniform.

The spherical like particles are not visible in any of the SEM micrographs. This suggests that the spherical particles are surrounded by the rod and needle like particles when in the powder- these were likely broken by the sonicating process during the preparation for TEM analysis.

To determine whether the samples displayed a phase change upon heating and to measure the thermochromic properties of the samples, variable temperature UV/Vis spectra were obtained (**Figure 7**). Samples as synthesised directly from the CHFS process (with no annealing) did not show a temperature induced phase change.

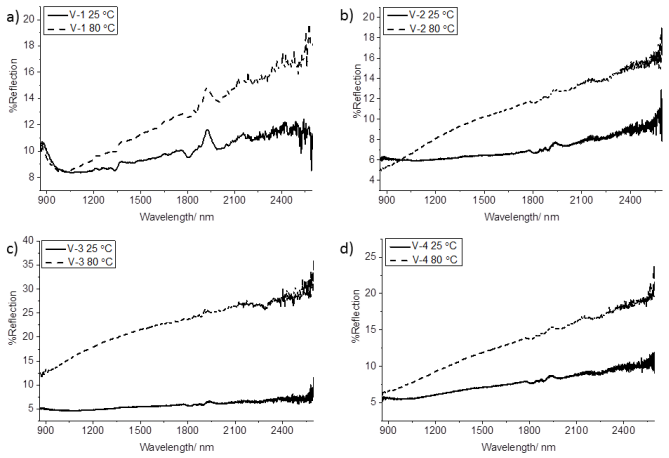

Figure 7: UV/Vis variable temperature reflectance spectra for **a)** V-1, **b)** V-2, **c)** V-3 and **d)** V-4. All samples were measured at 25 °C (bottom line) and 80 °C (top line).

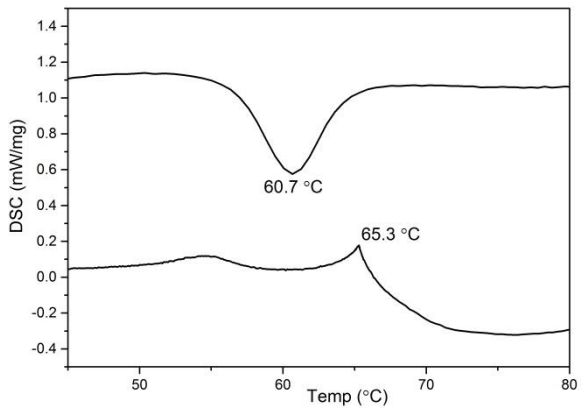

Figure 8: Typical Differential Scanning Calorimetry curve for VO_2 powder synthesised by continuous hydrothermal flow synthesis. The top curve shows the forward scan, with a large endothermic change as the MST phase transition occurs. The bottom curve shows the DSC trace for the reverse transition; here an exothermic curve is seen as the tetragonal to monoclinic phase change occurs.

All post-heat treated samples displayed an increase in reflectance when heated above the MST, which was the expected result if the material had been displaying a phase change from semi-conductor to semi-metallic. The sample that had the greatest reflectance change was sample V-3, which displayed a maximum of 25 % change in reflectance between the hot and cold spectra.

The sample that had the poorest thermochromic switch was sample V-1, which only displayed a maximum 8 % switch between the hot and cold spectra. The UV/Vis spectra correlate with the initial XRD data (**Figure 1a)**), sample V-3 was closest to the reference XRD pattern and sample V-1 was the least similar. This is further evidence that reaction temperature, for reactions with short residence times, is the most important factor for formation of monoclinic VO_2 nanoparticles in continuous hydrothermal flow synthesis.

To further elucidate the switching temperature and hysteresis loop of the heat treated VO_2 nanoparticles, differential scanning calorimetry (DSC) measurements were performed. **Figure 8** shows a typical curve for the samples synthesised. All samples showed a switch between 60-70 °C, with typical hysteresis loops of ~5 °C in all cases. Although it has been previously seen that particle size can affect the phase transition temperature, it can be seen from the SEM micrographs that the particle sizes are consistent at the surface, meaning that it would be expected that the samples synthesised in these experiments would be expected to show similar phase transition temperatures. The slight lowering of the MST temperature is attributed to strain in the nanoparticles.

There have been many previous reports on VO_2 nanoparticle synthesis. Gui *et al*. reported the formation of rod-like particles, using hydrazine and a 24-hour post-annealing treatment.[41] It was reported that the nano-rods were only observed at low reaction temperatures (150 °C for 2 days), these trends are reflected in this research where the lower reaction temperatures led to more rod-like morphologies. For future production, it would be expected that a CHFS process, such as used herein, would allow the same type of morphology to be produced using much safer chemicals on a much larger scale, and with a shorter post-annealing treatment. VO_2 rod-like morphologies have potential applications in batteries, where the VO_2 (B) phase is favoured due to its ability to intercalate lithium ions. Corr *et al*. have reported on both VO_2 (B) and (M) nano-rod morphologies.[28] The synthesis of the VO_2 nano-rods required a 24 hour hydrothermal treatment. An optimisied CHFS reaction would also be expected to form these rod-like structures in a fraction of this time, ~20 s.

Although VO_2 (B) was not the desired phase in this research, the initial results from both the XRD and Raman suggested that the material in certain samples was indeed a mixture of VO_2 (B) and (M) phases. This again suggests that a CHFS approach to the formation of VO_2 (B) nanoparticles, with a lowering of the mixing temperature, would yield a fast through-put method with the ability to tune the particle size, shape and growth by the reaction temperature and residence time in the reactor. As mentioned in the introduction, VO_2 (B) has been shown to have applications for battery technologies with the ability to intercalate lithium ions.

Previous methods for producing VO_2 (B) nanoparticles have been batch hydrothermal processes,[44-46] which are difficult to scale for industrial processes.

Li *et al*. have modelled different nano-particle shapes to elucidate the effect of morphology on the thermochromic response.[47, 48] It was noted that although rod-like morphologies could theoretically give a better thermochromic response than purely spherical particles, this is very dependent on the orientation of the particles in the relation to the incident radiation. This would give an explanation as to why sample V-3, which only contained spherical particles, gave the best response. The orientation of the nano-particles in the films used for the functional testing was not determined. The spherical particles would give the same response regardless of the angle of the incident radiation, whereas the nano-rods could potentially give differing responses if they were aligned.[48, 49]

Further studies could be conducted to try to reduce the size of the nanoparticles formed by changing the nature of the precursor,[50, 51] concentration of the precursor solution,[52] addition of surfactants,[53-55] doping,[56] mixing temperature[52] and residence time;[52] which have all been shown to have an effect on the size of the nanoparticles formed from CHFS processes.

Conclusions

A series of thermochromic VO_2 (M) nanoparticles, with varying morphologies, were synthesised by a continuous hydrothermal flow synthesis (CHFS) followed by a heat-treatment. Interestingly, VO_2 (B) nanoparticles were also found to be initially formed in some cases, which has applications for Li-ion battery materials. To the best of our knowledge, this is the first time that thermochromic VO_2 has been synthesised from such a continuous hydrothermal route. The particles are highly crystalline and show excellent thermochromic properties, with a fully reversible phase change at ~68 °C. The morphology of the particles was found to be dependent upon the reaction temperature, with residence time also being found to influence

particle growth. The CHFS route allows the synthesis of such particles on even larger scales, which could be of benefit in future industrial applications. Furthermore, the process offers the ability to tailor the size and morphology of the synthesised particles through independent control of reaction temperature and residence time, amongst other parameters, allowing for the modification of particles to suit a particular process whilst maintaining the desired properties.

Acknowledgements

Dr Steven Firth for assistance with SEM micrographs and DSC measurements and discussion of morphology of particles observed. Martin Vickers for assistance with collecting XRD patterns.

References

1 C. Change, IPCC, Geneva, Switzerland, 2007.
2 N. H. Stern, G. Britain and H. Treasury, *Stern Review: The economics of climate change*, HM treasury London, 2006.
3 A. Guisan, *Nature Clim. Change*, 2014, 4, 175-176.
4 U.-S. Buildings and C. Initiative, Paris: United Nations Environment Programme, 2007.
5 Y. Oka, T. Ohtani, N. Yamamoto and T. Takada, *Nippon seramikkusu kyokai gakujutsu ronbunshi*, 1989, 97, 1134-1137.
6 C. Huang, L. Chen, G. Xu and L. Miao, *J. Sol-Gel Sci. Technol.*, 2012, 63, 103-107.
7 L. Mai, Q. Wei, Q. An, X. Tian, Y. Zhao, X. Xu, L. Xu, L. Chang and Q. Zhang, *Advanced Materials*, 2013, 25, 2969-2973.
8 Y. Gao, C. Cao, L. Dai, H. Luo, M. Kanehira, Y. Ding and Z. L. Wang, *Energy Environ. Sci.*, 2012, 5, 8708-8715.
9 D. Munoz-Rojas and E. Baudrin, *Solid State Ionics*, 2007, 178, 1268-1273.
10 E. Baudrin, G. Sudant, D. Larcher, B. Dunn and J.-M. Tarascon, *Chemistry of Materials*, 2006, 18, 4369-4374.
11 M. Zhang and J. Dahn, *Journal of the Electrochemical Society*, 1996, 143, 2730-2735.
12 T. D. Manning, I. P. Parkin, R. J. H. Clark, D. Sheel, M. E. Pemble and D. Vernadou, *J. Mater. Chem.*, 2002, 12, 2936-2939.
13 S. M. Babulanam, T. S. Eriksson, G. A. Niklasson and C. G. Granqvist, *Sol. Energy Mater.*, 1987, 16, 347-363.
14 C. G. Granqvist, *Sol. Energy Mater. Sol. Cells*, 2007, 91, 1529-1598.
15 Y. Zhou, X. Chen, C. Ko, Z. Yang, C. Mouli and S. Ramanathan, *IEEE Electron Device Lett.*, 2013, 34, 220-222.
16 K. G. West, J. Lu, L. He, D. Kirkwood, W. Chen, T. P. Adl, M. S. Osofsky, S. B. Qadri, R. Hull and S. A. Wolf, *J. Supercond. Novel Magn.*, 2008, 21, 87-92.
17 J. M. Reyes, S. L. Segel and M. Sayer, *Can. J. Phys.*, 1976, 54, 1-8.
18 C. S. Blackman, C. Piccirillo, R. Binions and I. P. Parkin, *Thin Solid Films*, 2009, 517, 4565-4570.
19 S. Y. Li, G. A. Niklasson and C. G. Granqvist, *J. Appl. Phys.*, 2010, 108, 063525/063521-063525/063528.
20 J.-H. Son, J. Wei, D. Cobden, G. Cao and Y. Xia, *Chemistry of Materials*, 2010, 22, 3043-3050.
21 J. Zhou, Y. Gao, X. Liu, Z. Chen, L. Dai, C. Cao, H. Luo, M. Kanahira, C. Sun and L. Yan, *Physical Chemistry Chemical Physics*, 2013, 15, 7505-7511.
22 Y. Xu, W. Huang, Q. Shi, Y. Zhang, L. Song and Y. Zhang, *Journal of Sol-Gel Science and Technology*, 2012, 64, 493-499.
23 L. Mai, B. Hu, T. Hu, W. Chen and E. Gu, *The Journal of Physical Chemistry B*, 2006, 110, 19083-19086.
24 J. M. Booth and P. S. Casey, *Acs Applied Materials & Interfaces*, 2009, 1, 1899-1905.
25 Y. Li, S. Ji, Y. Gao, H. Luo and M. Kanehira, *Scientific reports*, 2013, 3.
26 T. Adschiri, K. Kanazawa and K. Arai, *Journal of the American Ceramic Society*, 1992, 75, 1019-1022.
27 C. J. Tighe, R. Q. Cabrera, R. I. Gruar and J. A. Darr, *Ind. Eng. Chem. Res.*, 2013, 52, 5522-5528.
28 S. A. Corr, M. Grossman, Y. Shi, K. R. Heier, G. D. Stucky and R. Seshadri, *Journal of Materials Chemistry*, 2009, 19, 4362-4367.
29 X. Wu, Y. Tao, L. Dong, Z. Wang and Z. Hu, *Materials Research Bulletin*, 2005, 40, 315-321.
30 R. I. Gruar, C. J. Tighe and J. A. Darr, *Ind. Eng. Chem. Res.*, 2013, 52, 5270-5281.
31 D. Sathyanarayana and C. Patel, *Bulletin of the Chemical Society of Japan*, 1964, 37, 1736-1740.
32 D. Sathyanarayana and C. Patel, *Bulletin of the Chemical Society of Japan*, 1967, 40, 794-797.
33 R. Li, S. Ji, Y. Li, Y. Gao, H. Luo and P. Jin, *Mater. Lett.*, 2013, 110, 241-244.
34 JP2013184091A, 2013.
35 J. Zhou, Y. Gao, X. Liu, Z. Chen, L. Dai, C. Cao, H. Luo, M. Kanahira, C. Sun and L. Yan, *Phys. Chem. Chem. Phys.*, 2013, 15, 7505-7511.
36 A. Magneli and G. Andersson, *Acta Chemica Scandinavica*, 1955, 9, 1378-1381.
37 U. Schwingenschlögl and V. Eyert, *Annalen der physik*, 2004, 13, 475-510.
38 T. D. Manning and I. P. Parkin, *Polyhedron*, 2004, 23, 3087-3095.
39 P. Schilbe, *Physica B: Condensed Matter*, 2002, 316, 600-602.
40 P. Schilbe and D. Maurer, *Materials Science and Engineering: A*, 2004, 370, 449-452.
41 W. Chen, J. Peng, L. Mai, H. Yu and Y. Qi, *Chemistry Letters*, 2004, 33, 1366-1367.
42 Z. Gui, R. Fan, W. Mo, X. Chen, L. Yang, S. Zhang, Y. Hu, Z. Wang and W. Fan, *Chemistry of Materials*, 2002, 14, 5053-5056.
43 T. Yao, L. Liu, C. Xiao, X. Zhang, Q. Liu, S. Wei and Y. Xie, *Angewandte Chemie*, 2013, 125, 7702-7706.
44 K. C. Kam and A. K. Cheetham, *Materials Research Bulletin*, 2006, 41, 1015-1021.
45 J. Nag and R. Haglund Jr, *Journal of Physics: Condensed Matter*, 2008, 20, 264016.
46 C. Nethravathi, C. R. Rajamathi, M. Rajamathi, U. K. Gautam, X. Wang, D. Golberg and Y. Bando, *Acs Applied Materials & Interfaces*, 2013, 5, 2708-2714.
47 F. Sediri, F. Touati and N. Gharbi, *Materials Science and Engineering: B*, 2006, 129, 251-255.
48 X. Li, X. Chen, X. Chen, C. Han and C. Shi, *Journal of Crystal Growth*, 2007, 309, 43-47.
49 S. Y. Li, G. A. Niklasson and C. G. Granqvist, *J. Appl. Phys.*, 2011, 109, 113515/113511-113515/113515.
50 S. Y. Li, G. A. Niklasson and C. G. Granqvist, *MRS Online Proc. Libr.*, 2011, 1315, No pp. given.
51 S. Y. Li, G. A. Niklasson and C. G. Granqvist, *Annu. Tech. Conf. Proc. - Soc. Vac. Coaters*, 2011, 54th, 29-34.
52 Y. Hakuta, T. Ohashi, H. Hayashi and K. Arai, *Journal of Materials Research*, 2004, 19, 2230-2234.
53 Y. Ding, G. Zhang, H. Wu, B. Hai, L. Wang and Y. Qian, *Chemistry of Materials*, 2001, 13, 435-440.
54 G. Amin, M. Asif, A. Zainelabdin, S. Zaman, O. Nur and M. Willander, *Journal of Nanomaterials*, 2011, 2011, 5.
55 P. Boldrin, A. K. Hebb, A. A. Chaudhry, L. Otley, B. Thiebaut, P. Bishop and J. A. Darr, *Ind. Eng. Chem. Res.*, 2007, 46, 4830-4838.

56 A. Sahraneshin, S. Asahina, T. Togashi, V. Singh, S. Takami, D. Hojo, T. Arita, K. Minami and T. Adschiri, *Crystal Growth & Design*, 2012, 12, 5219-5226.
57 X. Sun, X. Chen, Z. Deng and Y. Li, *Materials Chemistry and Physics*, 2003, 78, 99-104.
58 J. B. Goodall, S. Kellici, D. Illsley, R. Lines, J. C. Knowles and J. A. Darr, *Rsc Advances*, 2014, 4, 31799-31809.